An Ultra-Wideband High-Isolation Single-Antenna Full-Duplexer Based on Dual-Phase Cancellation

Jie XUE [1], Binbin SU [1], Yongcai LIU [1], Liang ZHOU [1] Jin MENG [1,2]

[1] National Key Laboratory of Electromagnetic Energy, Naval University of Engineering, No. 717 Jiefang Avenue, 430033 Wuhan, China
[2] Qianyuan Laboratory, No. 6 Courtyard Xiangshan Branch Lane Xihu District, 310024 Hangzhou, China

bin23@nue.edu.cn, 1901703@nue.edu.cn

Submitted February 7, 2026 / Accepted April 23, 2026 / Online first May 26, 2026

Abstract. *Wideband transmit-receive shared-antenna full-duplexers are a key technology for radar, communication, and electronic countermeasure systems. In special scenarios such as retrodirective cross-eye jamming, RF systems must adopt a TR shared-antenna architecture with a frequency coverage of 6–18 GHz. However, high-power signals leaking from the transmitter in this architecture interfere with the reception of useful signals at the receiver. To address this issue, this paper proposes an ultra-wideband high-isolation anti-symmetric duplexer. This duplexer is configured with one 180° hybrid coupler, one power divider, and two circulators. Based on a dual-phase cancellation mechanism, it theoretically enables complete suppression of self-interference signals induced by circulator leakage and antenna standing waves. Experimental results demonstrate that the proposed duplexer achieves Tx-Rx isolation exceeding 33 dB over the 6–18 GHz band. Compared with traditional duplex systems based on a single circulator and an orthogonal balanced network, the proposed design improves isolation by 13–22 dB. This work represents the first passive full-duplexer architecture to simultaneously cancel both circulator leakage and antenna reflections over the full 6–18 GHz band. This scheme can be extended to applications in retrodirective cross-eye jammers as well as other radio frequency systems that face wideband isolation problems.*

Keywords

Transmit-receive isolation, full-duplexer, ultra-wideband, retrodirective cross-eye jamming

1. Introduction

Wideband transmit-receive (TR) shared-antenna full-duplexers, known for their compact size, low cost, and simple structure, are fundamental components in RF systems such as electronic countermeasures, radar, and communications. In many practical applications, various radio frequency (RF) systems impose stringent requirements on full-duplexers. Take retrodirective cross-eye jamming [1], [2], a typical technology in the field of electronic countermeasures, as an example. It requires a TR shared-antenna full-duplex architecture to achieve stable jamming performance [3], [4]. Meanwhile, retrodirective cross-eye jammers need to cover a frequency range of 6−18 GHz or even wider to realize broadband response to radars operating in various frequency bands. However, this architecture has an inherent bottleneck: high-power signals leaking from the transmitter cause significant interference to the receiver's useful signals, severely degrading the system's receiving sensitivity [5], [6]. Therefore, improving the isolation of ultra-wideband full-duplex systems has become a critical challenge driving the development of retrodirective cross-eye jammers and various RF systems [6–8].

At present, scholars have conducted extensive research on full-duplexers with transmit-receive shared antennas. Early schemes mainly relied on ferrite circulators to achieve transmit-receive isolation, but their isolation was only 10−20 dB, which was insufficient for practical requirements. Against this background, full-duplexers based on balanced RF circuits have become a research focus due to their advantages such as low cost and passive cancellation [9–13].

Lim [9] proposes a front-end structure composed of balanced directional couplers and four-port fed antennas for Ultra-High Frequency (UHF) Radio-Frequency Identification (RFID) readers, which can achieve robust transmission leakage cancellation under load changes and antenna mutual coupling, with an isolation of 45–50 dB in the UHF band. Siu [10] utilizes three orthogonal couplers and two circulators in a balanced circuit, achieving 35 dB isolation across 10.2−12.8 GHz. Yang [11] further applies fractal theory to design an enhanced coupler group, achieving over 40 dB of isolation within a 500 MHz bandwidth centered at 2.4 GHz. Mahdi [12] proposes an improved self-interference canceller incorporating dual circulators, a Wilkinson power divider, and a wideband phase shifter. This canceller compensates for circulator mismatch using the phase shifter, achieving over 40 dB isolation in 9.6−10.2 GHz. Nawaz [13] presents a dual-

DOI: 10.13164/re.2026.0315

polarized microstrip patch antenna scheme using 180°ring hybrid coupler differential feeding, with a peak isolation exceeding 67 dB over the narrow 2.4 GHz band. Zhang [14] introduces a single-antenna full-duplex subsystem with a high-isolation network (two orthogonal hybrid couplers + two circulators) and a dual-fed stacked patch antenna, achieving >50 dB isolation across 2.018−2.12 GHz.

However, the isolation bandwidth of the balanced schemes mentioned above is relatively narrow (mostly narrowband or broadband within one octave), which cannot cover the ultra-wideband requirement of 6−18 GHz. In addition, some scholars have attempted to suppress transmit-receive shared-antenna interference through polarization isolation [15–19]. To ensure cross-eye jamming effectiveness, cross-eye jamming signals require a high Jammer-to-Signal Ratio (JSR), where a minimum of $JSR \geq 20$ is typically required [20]. Orthogonal polarization leads to a significant reduction in the intensity of the jamming signal received by the jammed radar, which fails to meet the JSR requirement. Therefore, polarization isolation technology is not suitable for retrodirective cross-eye jammers.

This paper proposes an ultra-wideband (UWB) anti-symmetric full-duplexer with high isolation to address the Tx–Rx isolation challenge in UWB RF systems such as retrodirective cross-eye jammers. The study proceeds through theoretical analysis, circuit design, and experimental verification: 1) the working principle and isolation constraints of traditional full-duplexers are analyzed; 2) the structure and core device selection of the anti-symmetric full-duplexer are presented; and 3) the effectiveness and superiority of the proposed scheme are validated via comparative experiments with conventional full-duplex systems. The proposed design advances the state of the art in two fundamental respects. First, it introduces a dual-phase cancellation topology capable of simultaneously suppressing both circulator leakage and antenna standing waves, a capability that conventional balanced architectures do not offer. Second, it demonstrates a passive full-duplexer covering the entire 6–18 GHz band with a measured isolation exceeding 33 dB, which represents a 13–22 dB improvement over re-tested single-circulator and balanced orthogonal network benchmarks.

2. Analysis of Isolation Performance of Traditional Full-Duplexers

2.1 Single-Circulator-Based Full-Duplexer

In single-antenna full-duplex systems, the scheme based on a single circulator is the most commonly used full-duplex architecture. A circulator is a microwave passive component with unidirectional transmission characteristics. Its operation relies on the gyromagnetic effect of ferrite materials. It enables directional port separation between transmitted and received signals.

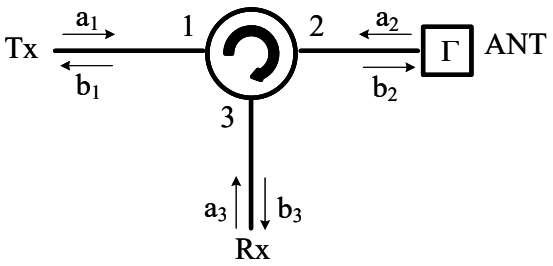

Fig. 1. Schematic diagram of the full-duplexer based on a single circulator. a_i denotes the incident signal at the i-th port, and b_i denotes the emergent signal at the i-th port ($i = 1, 2, 3$).

The structure of the full-duplexer based on a single circulator is illustrated in Fig. 1, and its signal transmission paths are described as follows: the transmitted signal is input through Port 1 of the circulator and subsequently output to the antenna via Port 2, while the signal received by the antenna is routed to the receiver through Port 3 of the circulator.

For an ideal circulator (with perfect port matching and a port reflection coefficient of 0), its scattering matrix (S-matrix) can be expressed as [9]:

$$\mathbf{S} = \begin{bmatrix} 0 & \beta & \alpha \\ \alpha & 0 & \beta \\ \beta & \alpha & 0 \end{bmatrix} \tag{1}$$

where α and β are the forward and reverse transmission coefficients, respectively.

The self-interference signal at the receiver (Port 3) consists of two components: direct circulator leakage βa_1 and antenna-reflected leakage $\alpha^2 \Gamma a_1$, where Γ is the antenna reflection coefficient. Therefore, the leakage ratio of Port 3 is:

$$\frac{b_3}{a_1} = \beta + \alpha^2 \Gamma \tag{2}$$

where (2) shows that the isolation performance depends on β, α and Γ.

To quantitatively evaluate the system isolation capability, the intrinsic isolation of the circulator, denoted I_c (in dB), is defined as the power ratio between forward and reverse transmission:

$$I_c = 10\log_{10}\left(\frac{|\alpha|^2}{|\beta|^2}\right). \tag{3}$$

For wideband linear frequency modulated (LFM) signals, the direct circulator leakage and the antenna-reflected leakage experience different electrical lengths, resulting in distinct instantaneous frequencies at the same time instant and thus exhibiting non-coherent characteristics. Consequently, the power levels of the two interference components can be summed directly, and the total isolation of the full-duplexer I (in dB) is approximated as

$$I = -10\log_{10}\left(|\beta|^2 + |\alpha^2 \Gamma|^2\right). \tag{4}$$

In practical circulators, the forward insertion loss is negligibly small, so that $|\alpha| \approx 1$. Under this approximation,

the squared magnitude of the reverse transmission coefficient follows directly from (3). Substituting these approximated quantities into (4) and incorporating the standard relationship between Γ and VSWR leads to the final design expression

$$I \approx -10\log_{10}\left(10^{-I_c/10} + \left(\frac{\mathrm{VSWR}-1}{\mathrm{VSWR}+1}\right)^2\right). \tag{5}$$

Figure 2 presents the isolation characteristics of the full-duplexer computed from (5), from which the following observations can be drawn:

1. The system isolation I increases as the antenna VSWR decreases and as the circulator intrinsic isolation I_c increases.

2. To achieve $I \geq 30$ dB, two conditions must be satisfied simultaneously: $I_c \geq 30$ dB and VSWR ≤ 1.1.

Although the isolation performance of the single-circulator full-duplexer can be improved by increasing the circulator' s intrinsic isolation I_c and reducing the antenna VSWR, there are significant limitations in engineering practice. On the one hand, the intrinsic isolation of commercial circulators is mostly 10–20 dB, making it difficult to achieve $I_c \geq 30$ dB. On the other hand, the VSWR of wideband antennas is typically 1.5–2.5, which cannot meet the stringent condition of VSWR ≤ 1.1. These limitations render the single-circulator scheme inadequate for retrodirective cross-eye jammers.

2.2 Balanced Orthogonal Network-Based Full-Duplexer

To overcome the performance bottleneck of the single-circulator scheme, researchers have proposed many full-duplexer designs based on balanced RF circuits. Among these, the balanced orthogonal network-based full-duplexer (BNF) is a typical balanced RF circuit scheme [9–11]. Composed of three 3 dB hybrid couplers and two circulators, this scheme suppresses direct circulator leakage through phase cancellation. As shown in Fig. 3, the BNF-based full-duplexer [10] operates as follows:

1. A 3 dB hybrid coupler splits the transmitted signal into two equal-amplitude in-phase and quadrature (I/Q) orthogonal signals.

2. After forward propagation through the circulators, these two signals are combined into an equal-amplitude in-phase signal by another 3 dB hybrid coupler, which is then transmitted via the antenna.

3. Meanwhile, the two orthogonal signals leak backward through the circulators and are converted into equal-amplitude anti-phase signals by the 3 dB hybrid coupler; these signals are superimposed and canceled out at the receiving port.

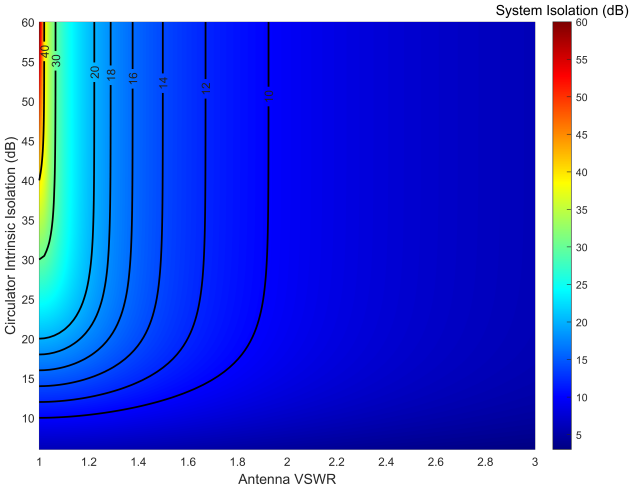

Fig. 2. Heatmap of isolation I of single-circulator full-duplexer vs. antenna VSWR and circulator intrinsic isolation I_c.

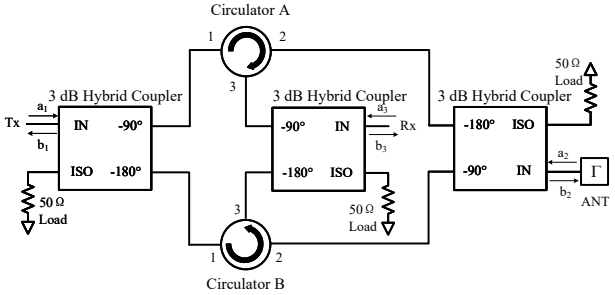

Fig. 3. Schematic diagram of the full-duplexer based on a balanced orthogonal network.

Assuming the 3 dB hybrid couplers are ideal components and the circulator ports are matched, the S-matrix of the circuit is [10]:

$$\mathbf{S} = \frac{\mathrm{j}}{2}\begin{bmatrix} 0 & \beta_A+\beta_B & \alpha_A-\alpha_B \\ \alpha_A+\alpha_B & 0 & \beta_A+\beta_B \\ \beta_A-\beta_B & \alpha_A+\alpha_B & 0 \end{bmatrix} \tag{6}$$

where α_A and β_A are the forward and reverse transmission coefficients of Circulator A, respectively. α_B and β_B are the forward and reverse transmission coefficients of Circulator B, respectively.

From (6), the leakage ratio from the transmitter end to the receiver end can be derived as [10]:

$$\frac{b_3}{a_1} = -\frac{1}{2}(\beta_A-\beta_B) - \frac{1}{2}\left(\alpha_A^2+\alpha_B^2\right)\Gamma. \tag{7}$$

When Circulators A and B have identical RF performance ($\alpha_A = \alpha_B = \alpha, \beta_A = \beta_B = \beta$), Equation (7) simplifies to [10]

$$\frac{b_3}{a_1} = -\alpha^2\Gamma. \tag{8}$$

From (7)–(8), it is evident that device consistency is critical to improving the performance of the full-duplexer. When the circulators have consistent performance, the leakage signals from the circulators can be completely canceled. However, in the BNF-based full-duplexer, the reverse leakage signal from the antenna cannot be eliminated, which becomes the core bottleneck restricting further improvement of isolation.

3. Design and Implementation of the Anti-Symmetric Full-Duplexer

Section 2 analysis indicates that the isolation performance of the single-circulator architecture is constrained by both the device's inherent isolation and antenna standing waves. Traditional phase cancellation architectures, typified by the balanced orthogonal network, can only suppress circulator reverse leakage but fail to eliminate antenna standing waves, which constitutes the core bottleneck for achieving ultra-wideband high isolation. To overcome this technical limitation and address the common transceiver isolation requirements of 6−18 GHz ultra-wideband RF systems, an anti-symmetric full-duplexer is proposed in this section. Through topological innovation, the conventional single-phase cancellation mechanism is enhanced to a dual-phase cancellation mechanism, enabling simultaneous cancellation of both circulator reverse leakage and antenna standing waves. This section will sequentially present the theoretical analysis, circuit implementation, and RF link consistency verification of the proposed architecture.

3.1 Theoretical Analysis of the Anti-Symmetric Full-Duplexer

The structure of the proposed anti-symmetric full-duplexer is shown in Fig. 4. It comprises one 180° hybrid coupler, one Wilkinson power divider, and two circulators (A and B). The signal paths of this full-duplexer are divided into three categories: transmission, reception, and cancellation, which are detailed as follows:

1. Transmission path: The transmitted signal is split by the 180° hybrid coupler into two equal-amplitude, opposite-phase signals. One signal propagates forward through Circulator A and is radiated via the antenna, while the other propagates forward through Circulator B and is fed to the duplicate antenna.

2. Reception path: The external useful signal received by the antenna is transmitted forward through Circulator A to the Wilkinson Power Divider. Since Circulator B is connected to the duplicate antenna (with no additional received signal input), the power divider transmits the useful signal to the receiver.

3. Cancellation path: Self-interference cancellation is achieved via dual-phase cancellation. Firstly, the two reverse leakage signals from Circulators A and B are equal in amplitude and opposite in phase, and they cancel each other out after being combined by the power divider. Secondly, the reflected signals from the transmitting antenna and the duplicate antenna are transmitted forward to the power divider through Circulators A and B, respectively. If the reflection coefficients of the two antennas are consistent ($\Gamma_1 = \Gamma_2$), these reflected signals also superimpose and cancel each other.

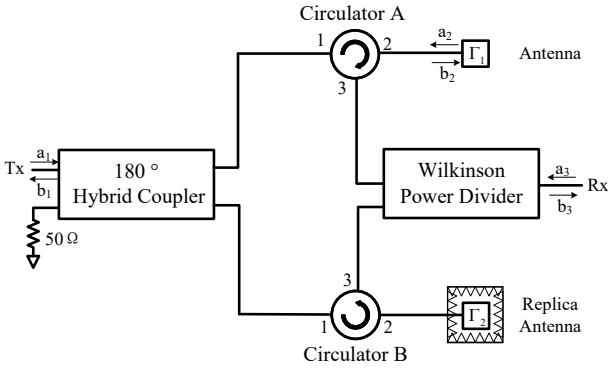

Fig. 4. Schematic diagram of the anti-symmetric full-duplexer.

Assuming the 180° hybrid coupler and power divider are ideal components and the circulator ports are matched, the S-matrix of the system is expressed as:

$$\mathbf{S} = -\begin{bmatrix} 0 & \frac{-\beta_a}{\sqrt{2}} & \frac{\beta_b}{\sqrt{2}} & \frac{\mathrm{j}(\alpha_a-\alpha_b)}{2} \\ \frac{-\alpha_a}{\sqrt{2}} & 0 & 0 & \frac{\mathrm{j}\beta_a}{\sqrt{2}} \\ \frac{-\alpha_b}{\sqrt{2}} & 0 & 0 & \frac{\mathrm{j}\beta_b}{\sqrt{2}} \\ \frac{\mathrm{j}(\beta_a-\beta_b)}{2} & \frac{\mathrm{j}\alpha_a}{\sqrt{2}} & \frac{\mathrm{j}\alpha_b}{\sqrt{2}} & 0 \end{bmatrix}. \tag{9}$$

From (9), the leakage ratio from the transmitter to the receiver is derived as:

$$\frac{b_4}{a_1} = -\frac{1}{2}\mathrm{j}\left(\beta_a - \beta_b\right) - \frac{1}{2}\mathrm{j}\left(\Gamma_1\alpha_a^2 - \Gamma_2\alpha_b^2\right) \tag{10}$$

where Γ_1 is the reflection coefficient of the transmitting antenna, and Γ_2 is the reflection coefficient of the duplicate antenna. When Circulators A and B have consistent RF performance ($\alpha_\mathrm{A} = \alpha_\mathrm{B} = \alpha$, $\beta_\mathrm{A} = \beta_\mathrm{B} = \beta$), Equation (10) simplifies to:

$$\frac{b_4}{a_1} = \frac{1}{2}\mathrm{j}\alpha^2\left(\Gamma_1 - \Gamma_2\right). \tag{11}$$

From (11), the following conclusions can be drawn. First, when the circulators exhibit consistent performance, reverse leakage from the circulators can be completely canceled. Second, when the reflection coefficients of the two antennas are consistent ($\Gamma_1 = \Gamma_2$), antenna standing waves can also be completely suppressed. Furthermore, when both conditions are satisfied, the theoretical isolation of the system approaches infinity.

3.2 Circuit Implementation of the Anti-Symmetric Full-Duplexer

The physical structure of the anti-symmetric full-duplexer is shown in Fig. 5. All RF components are commercial off-the-shelf products from Suzhou Talent Microwave Company, with a frequency range covering 6–18 GHz. The specific component selection is as follows:

1. Circulator: Model TLC60180-S;

2. 180° Hybrid Coupler: Model TBG-40180-3S-180S;

3. Wilkinson Power Divider: Model RS2W20180-S.

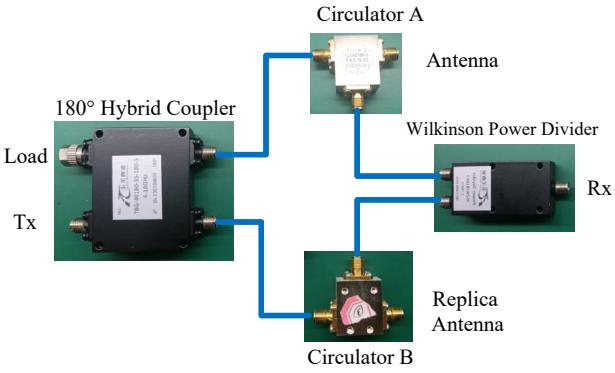

Fig. 5. Physical structure of the anti-symmetric full-duplexer.

The cancellation effect of the anti-symmetric structure depends on the consistency of the RF links. Therefore, during circuit construction, the electrical parameter differences between the symmetric paths must be strictly controlled by adhering to the following principles:

1. RF cables of the same model (with a characteristic impedance of 50 Ω) are used to connect components, which ensures the consistent electrical length of the symmetric links.
2. Symmetric components (Circulators A/B, RF cables) are arranged symmetrically when connected via RF lines to reduce the impact of temperature drift and mechanical stress differences on component consistency.

3.3 Tests of Component Consistency

To quantify the consistency between the two symmetric RF branches, we measured their S-parameters using a vector network analyzer (VNA, Keysight N5227B). The test frequency range was 6–18 GHz with an input power of −5 dBm, according to the following steps:

1. Test for Branch A: The input port of the 180° hybrid coupler was connected to the signal port of the VNA (simulating the transmitter, Tx), while its 180° output port was connected to Port 1 of Circulator A. The isolation port and 0° output port of the 180° hybrid coupler were terminated with 50 Ω loads. Port 2 of Circulator A was terminated with a 50 Ω load, and Port 3 of Circulator A was connected to Splitter Port 1 of the power divider. Splitter Port 2 of the power divider was terminated with a 50 Ω load, and the combiner port of the power divider was connected to the receiving port of the VNA (simulating the receiver, Rx). The S-parameters for branch A, denoted as S_A, were recorded.
2. Test for Branch B: The input port of the 180° hybrid coupler was connected to the signal port of the VNA (simulating the transmitter, Tx), while its 180° output port was connected to Port 1 of Circulator B. The isolation port and 0° output port of the 180° hybrid coupler were terminated with 50 Ω loads. Port 2 of Circulator B was terminated with a 50 Ω load, and Port 3 of Circulator B was connected to splitter Port 1 of the power divider. Splitter Port 2 of the power divider was terminated with a 50 Ω load, and the combiner port of the power divider was connected to the receiving port of the VNA (simulating the receiver, Rx). S-parameter, S_B, was acquired by scanning.

The measured S-parameters of the two symmetric branches are shown in Fig. 6. It should be noted that the measured S-parameters included 3 dB of inherent attenuation introduced by the splitting of the 180° hybrid coupler and 3 dB of inherent attenuation introduced by the combining of the power divider, resulting in a total attenuation of 6 dB. Within the 6–16 GHz band, the two branches exhibited excellent consistency. The maximum amplitude difference was less than 1.5 dB. The maximum deviation of the phase difference from the ideal value (180°) was less than 9°. And the branch insertion loss was less than 25 dB. In contrast, within the 16–18 GHz band, the branch consistency deteriorated significantly. The maximum amplitude difference reached 5.1 dB, the maximum deviation of the phase difference from the ideal value (180°) reached 19°, and the peak insertion loss of the branches exceeded 32 dB. The consistency of the two branches was mainly affected by the combined effects of the reverse leakage difference between the two circulators and the standing wave fluctuation of the 50 Ω loads. Furthermore, the temperature drift of device parameters and parasitic effects in the high-frequency band exacerbated the degradation of device performance consistency.

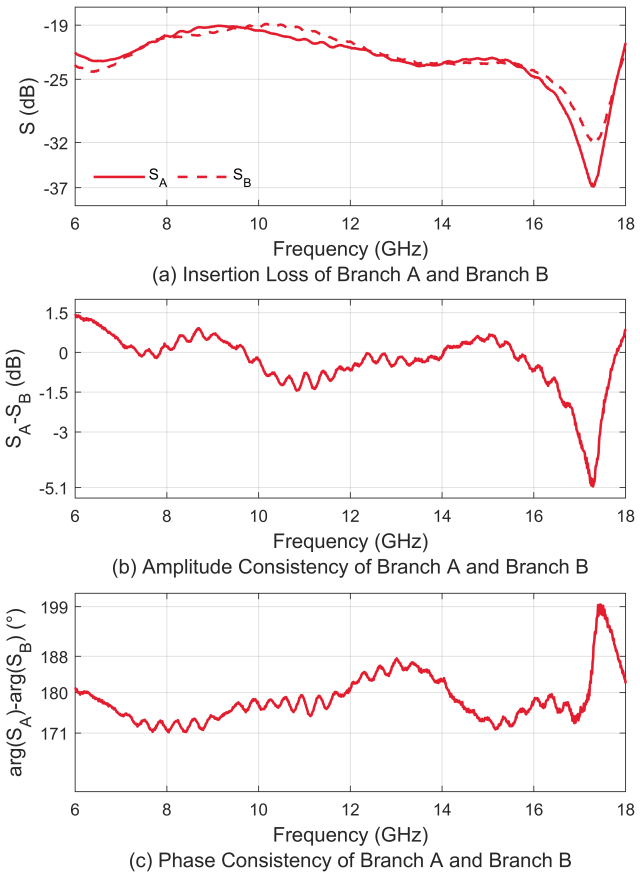

Fig. 6. Measured S-parameters of RF branches A and B.

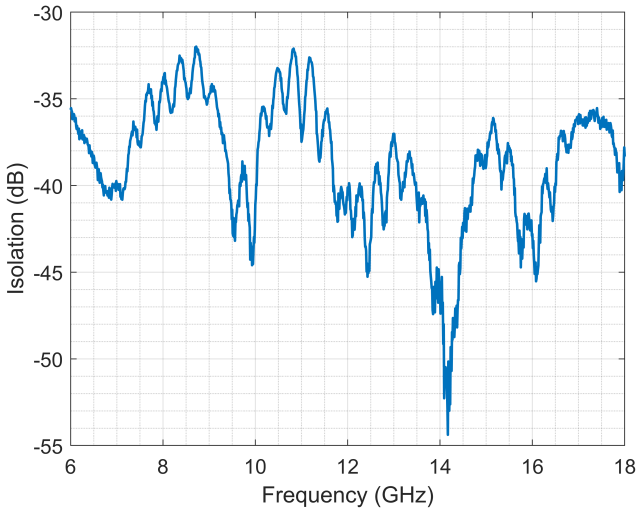

Fig. 7. Theoretical isolation frequency response curve of the anti-symmetric full-duplexer based on the measured S-parameters.

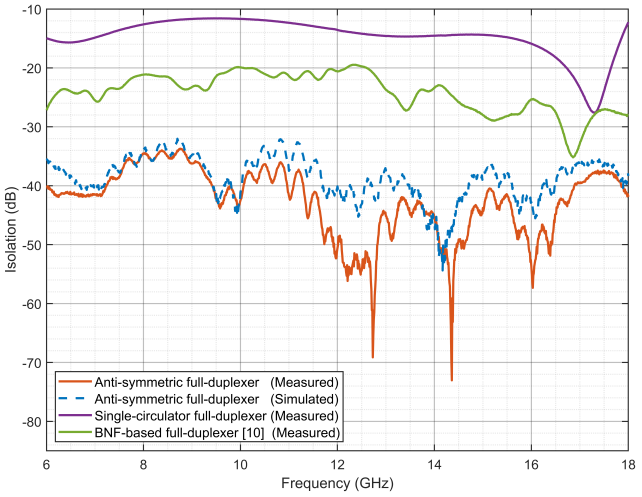

Fig. 8. Measured transmit–receive isolation of the three full-duplex systems vs. frequency (6–18 GHz).

Overall, the forward consistency performance of the two circulators was superior to their reverse consistency performance, with better consistency observed in the 6–16 GHz band where the forward insertion loss was relatively lower. The reverse consistency was primarily limited by the combined effects of direct circulator leakage and standing waves of the 50 Ω load.

Based on the phase cancellation principle of the anti-symmetric structure and the measured S-parameters, the calculation formula for the isolation I of the full-duplexer is derived as:

$$I = 20\log_{10}\left(\sqrt{2}\,|S_{\mathrm{A}} + S_{\mathrm{B}}|\right). \tag{12}$$

The frequency response curve of the theoretical isolation for the full-duplexer, plotted using (12), is shown in Fig. 7. It can be observed that within the 6–16 GHz band, the symmetric branches of the full-duplexer have low insertion loss and good consistency. Thus, the self-interference anti-phase cancellation mechanism functions sufficiently, leading to a theoretical isolation greater than 32 dB. Within the 16–18 GHz band, although the consistency of the symmetric branches decreases, the isolation still remains above 30 dB due to the increased insertion loss of the branches themselves.

4. System Performance Testing and Analysis

To verify the advantages of the anti-symmetric full-duplexer, two reference full-duplex systems were constructed using the same RF components. The first reference configuration was a single-circulator full-duplex system. The second was the balanced orthogonal network full-duplexer [10]. The BNF system employed a TBG-60280-3S90 3 dB hybrid coupler. A Keysight N5227B vector network analyzer was used to conduct comparative measurements of the transmit–receive isolation for the three full-duplex systems.

As a validation benchmark, the theoretical isolation curve derived from the branch S-parameters via (12) inherently accounts for all parasitic effects introduced during physical assembly, including connector discontinuities and cable phase imbalances. This provides a rigorous reference without the need for a separate full-wave electromagnetic simulation.

To eliminate interference from non-circuit factors such as antenna radiation and spatial multipath, and to ensure that the test data reflected only the isolation performance of the circuit itself, all antennas (transmit–receive and duplicate antennas) were replaced with 50 Ω loads. The remaining test conditions were set as follows: frequency range 6–18 GHz, step interval 10 MHz, and input power −5 dBm.

Figure 8 shows the measured transmit–receive isolation as a function of frequency for the three full-duplex systems, where the dashed line represents the theoretical isolation curve of the proposed anti-symmetric full-duplexer obtained from (12). As shown, the measured isolation curve of the anti-symmetric full-duplexer is in good agreement with its theoretical counterpart. The anti-symmetric full-duplexer exhibited transmit–receive isolation greater than 33 dB across the entire 6–18 GHz band, with isolation exceeding 40 dB in the 6–7.2 GHz and 11.3–16.9 GHz sub-bands. In comparison, the full-duplex system based on a single circulator was affected by circulator reverse leakage and load standing waves, yielding a measured isolation of just over 11 dB. The BNF-based full-duplex system [10] canceled the circulator leakage signal but failed to suppress load standing-wave interference, resulting in a measured isolation of only about 20 dB.

To provide a systematic comparison with state-of-the-art schemes, Table 1 summarizes the key performance metrics of existing classical full-duplexers, together with the re-tested single-circulator and BNF-based duplexers under identical conditions. As shown, most prior works [9–14] operate either below 3 GHz or within narrow sub-bands (e.g.,

Reference	Bandwidth [GHz]	Isolation [dB]	Limitation (principle)
[9]	0.86–0.96	45–50	Balanced coupler + 4-port antenna; UHF narrowband only, not applicable to 6–18 GHz
[10]	10.2–12.8	~35	Balanced orthogonal network; cannot cancel antenna reflection; poor wideband scalability
[11]	2.15–2.65	>40	Fractal enhanced coupler group; cannot cancel antenna reflection; poor wideband scalability
[12]	9.6–10.2	>40	Dual-circulator + Wilkinson + phase shifter; cannot cancel antenna reflection; poor wideband scalability
[13]	2.4	>67	Polarization isolation; requires orthogonal polarization, not suitable for cross-eye jamming
[14]	2.018–2.12	>50	Orthogonal hybrid + dual-fed patch; narrow bandwidth
Single circulator	6–18	>11	Inherent leakage plus antenna reflection; low isolation
This work	**6–18**	**>33**	**Requires duplicate antenna for standing-wave cancellation**

Tab. 1. Performance comparison of the proposed duplexer with existing schemes.

10.2–12.8 GHz in [10]), and those rated for 6–18 GHz (single circulator and BNF) exhibit poor wideband scalability, with measured isolation below 20 dB across the full band due to uncanceled antenna reflections or narrowband optimization. In contrast, the proposed anti-symmetric duplexer achieves >33 dB isolation over the entire 6–18 GHz range, a 13–22 dB improvement over traditional architectures. This advantage stems from the dual-phase cancellation mechanism, which suppresses both circulator leakage and antenna standing waves simultaneously.

The core advantage of the anti-symmetric full-duplexer lies in its dual-phase cancellation mechanism, which simultaneously cancels circulator leakage and suppresses antenna standing waves. Consequently, it achieves isolation performance significantly superior to that of traditional schemes across the entire ultra-wideband. It should be noted that the measurements were performed with 50 Ω loads instead of actual antennas to exclude radiation effects. In practical deployments, antenna VSWR may vary, and further validation with actual antenna loads would be beneficial.

5. Conclusions

This paper has presented an ultra-wideband high-isolation anti-symmetric full-duplexer whose key innovation is a dual-phase cancellation topology that simultaneously suppresses both circulator leakage and antenna standing waves. Experimental results demonstrate that the fabricated duplexer achieved a transmit–receive isolation greater than 33 dB across the entire 6–18 GHz band, with isolation exceeding 40 dB in the 6–7.2 GHz and 11.3–16.9 GHz subbands. Under identical test conditions, the proposed design improves isolation by at least 22 dB and 13 dB over the single-circulator and balanced orthogonal network schemes, respectively. These results confirm that the dual-phase cancellation mechanism provides a scalable passive solution for ultra-wideband shared-antenna systems, applicable to retrodirective cross-eye jammers, wideband radar, and electronic warfare front-ends.

Conflict of Interest

The authors declare no potential conflict of interests.

Acknowledgments

This work was supported in part by the National Key Research and Development Program of China under Grant 2021YFF1500100, in part by the National Natural Science Foundation of China under Grant 62001498, and by the Qianyuan Laboratory Project (S-KYZZ-F-02-202506-0060).

References

[1] LI, D., LIU, Y., ZHOU, L., et al. The impacts of phase noise on a long-baseline cross-eye jammer. *AEU - International Journal of Electronics and Communications*, 2024, vol. 185, p. 1–8. DOI: 10.1016/j.aeue.2024.155422

[2] LIU, Y., ZHOU, L., HE, F., et al. Probabilistic analysis of the amplitude-phase error tolerance for cross-eye jamming. *IEEE Transactions on Aerospace and Electronic Systems*, 2023, vol. 59, no. 1, p. 678–684. DOI: 10.1109/TAES.2022.3186968

[3] YANG, H., LIU, Y., LI, D., et al. An amplitude-phase measurement method for cross-eye jammers. *IEEE Transactions on Instrumentation and Measurement*, 2023, vol. 72, p. 1–9. DOI: 10.1109/TIM.2023.3325517

[4] YANG, H., LIU, Y., ZHOU, L., et al. The effect of excitation errors on the performance of AESA-based cross-eye jammers. *IEEE Antennas and Wireless Propagation Letters*, 2024, vol. 23, no. 3, p. 955–959. DOI: 10.1109/LAWP.2023.3340194

[5] LI, D., LIU, Y., ZHOU, L., et al. Platform echo and cross-eye jamming against active-passive composite monopulse radars. *IET Radar, Sonar & Navigation*, 2024, vol. 18, no. 6, p. 1025–1034. DOI: 10.1049/rsn2.12636

[6] LIU, T., LIAO, D., WEI, X., et al. Performance analysis of multiple-element retrodirective cross-eye jamming based on linear array. *IEEE Transactions on Aerospace and Electronic Systems*, 2015, vol. 51, no. 3, p. 1867–1876. DOI: 10.1109/TAES.2015.140874

[7] XING, J., GE, S., HE, F., et al. Design and analysis of heterodyne self-interference RF adaptive cancellation systems. *IEEE Transactions on Electromagnetic Compatibility*, 2025, vol. 67, no. 4, p. 1084–1094. DOI: 10.1109/TEMC.2025.3560147

[8] ZHANG, J., HE, F., LI, W., et al. Self-interference cancellation: A comprehensive review from circuits and fields perspectives. *Electronics*, 2022, vol. 11, no. 2, p. 1–23. DOI: 10.3390/electronics11020172

[9] LIM, W.-G., PARK, S.-Y., SON, W.-I., et al. RFID reader front-end having robust TX leakage canceller for load variation. *IEEE Transactions on Microwave Theory and Techniques*, 2009, vol. 57, no. 5, p. 1348–1355. DOI: 10.1109/TMTT.2009.2017308

[10] CHEUNG, S. K., HALLORAN, T. P., WEEDON, W. H., et al. MMIC-based quadrature hybrid quasi-circulators for simultaneous transmit and receive. *IEEE Transactions on Microwave Theory and Techniques*, 2010, vol. 58, no. 3, p. 489–497. DOI: 10.1109/TMTT.2010.2040325

[11] YANG, P., LIU, Y., QIN, F. Full-duplex self-interference cancellation method based on enhanced microstrip coupler group. *Journal of Microwaves*, 2024, vol. 40, no. 4, p. 24–29. DOI: 10.14183/j.cnki.1005-6122.202404006

[12] MAHDI, M., DARWISH, M., TORK, H., et al. An improved self-interference canceller for X-band radar transceivers. *IET Microwaves, Antennas & Propagation*, 2021, vol. 15, no. 9, p. 1381–1392. DOI: 10.1049/mia2.12177

[13] NAWAZ, H., TEKIN, I. Dual-polarized, differential-fed microstrip patch antennas with very high interport isolation for full-duplex communication. *IEEE Transactions on Antennas and Propagation*, 2017, vol. 65, no. 12, p. 7355–7360. DOI: 10.1109/TAP.2017.2765829

[14] ZHANG, L., LV, M., ZHANG, Z.-Y., et al. A single-antenna full-duplex subsystem with high isolation and high gain. *IEEE Open Journal of Antennas and Propagation*, 2024, vol. 5, no. 3, p. 620–625. DOI: 10.1109/OJAP.2024.3376568

[15] SIM, C.-Y.-D., CHANG, C.-C., ROW, J.-S. Dual-feed dual-polarized patch antenna with low cross-polarization and high isolation. *IEEE Transactions on Antennas and Propagation*, 2009, vol. 57, no. 10, p. 3321–3324. DOI: 10.1109/TAP.2009.2028702

[16] HAO, R. S., CHENG, Y. J., WU, Y. F., et al. A W-band low-profile dual-polarized reflectarray with integrated feed for in-band full-duplex application. *IEEE Transactions on Antennas and Propagation*, 2021, vol. 69, no. 11, p. 7222–7230. DOI: 10.1109/TAP.2021.3109641

[17] ZHANG, Y.-M., LI, J.-L. Differential-series-fed dual-polarized traveling-wave array for full-duplex applications. *IEEE Transactions on Antennas and Propagation*, 2020, vol. 68, no. 5, p. 4097–4102. DOI: 10.1109/TAP.2019.2948393

[18] ZHANG, Y.-M., ZHANG, S., LI, J.-L., et al. A dual-polarized linear antenna array with improved isolation using a slotline-based 180° hybrid for full-duplex applications. *IEEE Antennas and Wireless Propagation Letters*, 2019, vol. 18, no. 2, p. 348–352. DOI: 10.1109/LAWP.2019.2890983

[19] NAWAZ, H., TEKIN, I. Double-differential-fed, dual-polarized patch antenna with 90 dB interport RF isolation for a 2.4 GHz in-band full-duplex transceiver. *IEEE Antennas and Wireless Propagation Letters*, 2018, vol. 17, no. 2, p. 287–290. DOI: 10.1109/LAWP.2017.2786942

[20] LIU, T., LIU, Z., LIAO, D., et al. Platform skin return and multiple-element linear retrodirective cross-eye jamming. *IEEE Transactions on Aerospace and Electronic Systems*, 2016, vol. 52, no. 2, p. 821–835. DOI: 10.1109/TAES.2016.140949

About the Authors ...

Jie XUE received the B.S. degree in Communication Engineering from University of Science and Technology Beijing, Beijing, China, in 2019. He is currently pursuing the Ph.D. degree in Electrical Engineering at Naval University of Engineering, Wuhan, China. His current research interests include radar signal processing and electronic reconnaissance.

Binbin SU (corresponding author) received the Ph.D. Degree in Communication Systems from Lancaster University, Lancaster, U.K., in 2020. He is currently an Assistant Researcher with the Naval University of Engineering, Wuhan, China. His current research interests include radar signal processing and electronic reconnaissance.

Yongcai LIU received the Ph.D. degree in Information and Communication Engineering from the National University of Defense Technology, Changsha, China, in 2017. He is an Associate Researcher with the Naval University of Engineering, Wuhan, China. His current research interests include electronic countermeasures (ECM) and signal processing.

Liang ZHOU received the Ph.D. degree in Equipment Support from the Naval University of Engineering, Wuhan, China, in 2017. He is a Vice Professor with the Naval University of Engineering. His research interests include radar countermeasures and equipment support resource planning.

Jin MENG is a Professor and Doctoral Supervisor with the Naval University of Engineering. Dr. Meng is a recipient of the National Science Fund for Distinguished Young Scholars (NSFC). His research interests includ electromagnetic compatibility (EMC) and electronic countermeasures (ECM). He has published over 230 SCI/EI-indexed academic papers, and holds 65 patents.